Cellulose (2020) 27:4373–4387
https://doi.org/10.1007/s10570-020-03083-z

ORIGINAL RESEARCH

Mechanical and structural properties of cellulose nanofiber/poly(vinyl alcohol) hydrogels cross-linked by a freezing/thawing method and borax

H. Takeno · H. Inoguchi · Wen-Chuan Hsieh

Received: 31 August 2019 / Accepted: 24 February 2020 / Published online: 3 March 2020

Abstract The effect of cellulose nanofibers (CNFs) on the mechanical and structural properties of poly (vinyl alcohol) (PVA) hydrogels cross-linked dually by a freezing/thawing method and a cross-linker (borax) was investigated using tensile tests, FT-IR measurements and synchrotron simultaneous small-angle/wide-angle X-ray scattering (SAXS/WAXS). The cross-linking with borax and addition of CNF greatly improved the tensile performance of the PVA hydrogels prepared in the freezing/thawing method, e.g., the dual cross-linking resulted in remarkable increase in the fracture strain, the Young's modulus and the tensile strength. The fiber length effect on the mechanical properties of the CNF/PVA/borax hydrogels was examined, so that addition of CNF with longer fiber length increased the tensile modulus, whereas addition of CNF with shorter length caused extensibility higher than 1000% even at high CNF concentrations. SAXS/WAXS and FT-IR measurements have revealed that PVA was crystallized due to the freezing/thawing process, and both of PVA and CNF were cross-linked with borax, and hydrogen bonds between hydroxy groups of PVA (or/and CNF) were formed, indicating that the multiple cross-linking is effective for improvement of the tensile performance. In addition, the CNF/PVA/borax gel with the multi-physical cross-linking was found to possess the ability of the self-healing.

Keywords Cellulose nanofiber · Composite hydrogels · Synchrotron small-angle X-ray scattering · Highly stretchable · Poly (vinyl alcohol) · Freezing/thawing method

Electronic supplementary material The online version of this article (https://doi.org/10.1007/s10570-020-03083-z) contains supplementary material, which is available to authorized users.

H. Takeno (✉) · H. Inoguchi
Division of Molecular Science, Graduate School of Science and Technology, Gunma University, Kiryu, Gunma 376-8515, Japan
e-mail: takeno@gunma-u.ac.jp

H. Takeno
Gunma University Center for Food Science and Wellness, 4-2 Aramaki, Maebashi, Gunma 371-8510, Japan

W.-C. Hsieh
Department of Biological Science & Technology, College of Medicine, I-SHOU University, No. 8, Yida, Yanchao, Kaohsiung 82445, Taiwan, ROC

Introduction

Cellulose is the most abundant and sustainable biomaterials, and has been incorporated into polymers and rubbers as reinforcing agents. Reinforcement of polymers and rubbers can be achieved more efficiently by addition of nanocellulose (NC) such as cellulose nanocrystal (CNC) and cellulose nanofiber (CNF) that enables us to fabricate nanocomposite materials with

excellent mechanical performance, because miniaturization of cellulose fibers and cellulose crystals makes the dispersion of NC feasible (Wang et al. 2017; Xu et al. 2013).

Nanocomposite hydrogels containing a large amount of water are also attractive for potential application in a wide range of fields such as biomedical science (Hoffman 2012; Vashist et al. 2018), membrane (Cong et al. 2007), and actuators and sensors (Bauer et al. 2014; Chen and Pei 2017; Golmohammadi et al. 2017). In fact, incorporation of nanomaterials such as nanoparticles and nanofibers into polymer hydrogels has been widely used to improve the mechanical performance (Boyaci and Orakdogen 2016; De France et al. 2017; Takeno and Nakamura 2013). In most cases, the improvement can be accomplished, when the nanomaterials are well dispersed in the matrix and favorable interactions between the nanomaterials and polymer matrix exist (De France et al. 2017; Takeno and Kimura 2016). In the case of nanocellulose, it has some hydroxy groups in the repeating units, which can interact with various functional groups.

Poly(vinyl alcohol) (PVA), which is a water-soluble and biocompatible polymer, can be cross-linked chemically by the cross-linking agents such as glutaraldehyde (Lee et al. 2017) or physically by the micro-crystallites formed in the freezing–thawing (FT) process (Hassan and Peppas 2000a, b; Peppas 1975; Stauffer and Peppas 1992) and by complexing PVA with borate ions (Narita et al. 2013). In the FT process, water molecules crystallize with expelling PVA chains, which causes the more concentrated PVA region, so that crystallization of PVA is likely to occur (Holloway et al. 2013). Recent studies have shown that combination of multiple cross-linking has been effective for enhancement of mechanical performance. Lee et al. reported that the fracture stress of the hydrogel cross-linked by glutaraldehyde and by the FT method reached 12.6 MPa (1 FT cycle) and 18.3 MPa (5 FT cycles) (Lee et al. 2017). However, the fracture strain showed very low values of 34% (1 cycle) and 9.8% (5 cycles). Huang et al. fabricated PVA hydrogels cross-linked by borax, blending with polyvinylpyrrolidone (PVP) and a FT method (3 cycles). The compressive strength of the hydrogel with the best performance attained 1.8 MPa (80% compression) (Huang et al. 2017). However, no tensile tests were carried out in the literature.

It is a challenging subject to clarify the relationship between the mechanical properties and structure of the hydrogel with multiple-crosslinking because of the complex structure. Detailed structural analysis is necessary to characterize the hydrogel and understand the mechanism of high mechanical performance. Scanning electron microscopy (SEM) has been used as one of techniques to observe the structure of the hydrogel (Avolio et al. 2012, 2015). However, the process such as freeze-drying is necessary for the SEM observation of hydrogels, and the freezing process may influence the structure of the hydrogel (Hassan and Peppas 2000a, b). Thus, in-situ observation of the structure is more desirable for structural investigation of the hydrogel.

In-situ observation using simultaneous synchrotron small-angle X-ray scattering (SAXS) and wide-angle X-ray scattering (WAXS) are very effective to clarify structure of nanocomposites. Especially the synchrotron SAXS/WAXS measurements have been used to characterize structures of nanomaterials containing crystalline substances (Kaneko et al. 2013; Rath et al. 2014; Takeno 2016; Takeno et al. 2015). Thus, we believe that the SAXS/WAXS is one of the most suitable techniques to characterize CNF/PVA composite hydrogels. Our particular attention is to clarify the relationship between the mechanical properties and structure of the hydrogels from the structural analysis.

In this study, we investigated the mechanical and structural properties of PVA hydrogels cross-linked by a FT method and borax using tensile tests, simultaneous SAXS/WAXS and FT-IR techniques, and furthermore the effect of reinforcement of CNF on the PVA/borax hydrogels. In this paper, we shall show that the composite gels possess an excellent mechanical performance with high stretchability and self-healing ability.

Experimental

Materials

Three types of CNFs, IMa (polymerization degree of 800), WMa (polymerization degree of 650), and FMa (polymerization degree of 200) with different fibrous length were purchased from Sugino Machine Ltd. IMa, WMa and FMa are hereafter designated as CNF-

L, CNF-M and CNF-S, respectively. Poly (vinyl alcohol) (PVA) with weight-averaged molecular weight of 89,000–98,000 and hydrolysis higher than 99% from Sigma-Aldrich and sodium tetraborate decahydrate (Kanto Chemical Co. Inc.) were used in this study.

Preparation of CNF/PVA hydrogels

CNF and sodium tetraborate (borax) decahydrate were added to water in a vial, and afterwards the mixture was heated to 90 °C in order to dissolve borax. Furthermore, CNF was dispersed using an ultrasonic homogenizer (QSONICA, Model Q55) for 2 min at room temperature. In the case of the hydrogels without borax, after CNF was added to water in a vial, it was dispersed using the ultrasonic homogenizer for 2 min at room temperature. PVA was added to the mixture, and afterwards the vial was placed in the oil bath set at 90 °C for 60 min to dissolve PVA. The hydrogel prepared thus was placed in a stainless mold with a thickness of 1 mm, and was pressed for 10 s at ~ 65 °C. Then, after the hydrogel was placed in a refrigerator at − 20 °C for 1.5 h, it was thawed at room temperature for 1 day. The final concentrations of PVA and borax were 30 wt% and 1 wt%, respectively. The CNF-L, M, S were finally prepared at 1, 2, and 4 wt%.

Tensile tests

The samples (1 mm thickness) for tensile tests were cut with a dumbbell cutter (No.8, Kobunshi Keiki Co. Ltd.). The tests were performed at a speed of 10 mm/min, to obtain tensile stress (σ)-strain ($\Delta L/L_0$) curves, where σ was calculated with a cross-sectional area of the undeformed gel. ΔL and L_0 denote the deformation of the gel and the initial length before deformation, respectively. The elastic modulus (Young's modulus) E was estimated from a slope of the stress–strain curve at small strains. The average values of E, the fracture stress σ_f and the fracture strain ε_f were obtained from at least four measurements.

FT-IR

Fourier transform infrared spectroscopy (FT-IR, JASCO FT/IR 4700) was used to characterize the chemical structure of the hydrogels. The hydrogel prepared in the above manner was put in a stainless mold with a thickness of 0.5 mm, and then freeze-dried. Afterwards, the sample was further dried in a vacuum oven at 100 °C for ca. 12 h. The dried sample was measured by the attenuated total reflection (ATR) method.

Characterization of CNF

The samples of CNFs and the CNF composite hydrogels were observed under a field emission scanning electron microscope (FE-SEM Hitachi-4700, Japan). A completely dried blank sample was placed on a copper base, to which it was attached using conductive tape. This blank sample was then plated with platinum in a vacuum deposition machine, before being placed on the sample base of the FE-SEM for observation under an accelerating voltage of 10 kV at a working distance (WD) of 15 mm. The substances on the surface of the sample were then analyzed by energy dispersive spectroscopy (EDS) (HORIBA, Japan).

X-ray Diffraction (XRD) measurements were carried out to estimate crystallinity of CNF-L, M and S with an X-ray diffractometer (RIGAKU, RINT2200VF) using CuKα radiation at the Center for Instrumental Analysis of Gunma University. After the CNF dispersions were freeze-dried, the freeze-dried powder was filled in an aluminum spacer. The diffracted intensities were recorded in the range of 10°–60° at room temperature. The crystallinities of CNF-L, M and S were evaluated from the ratio between the area of crystalline reflection and the area of the whole diffraction profile.

Synchrotron SAXS/WAXS

Synchrotron simultaneous SAXS and WAXS measurements were performed at the beam line BL-6A at the photon factory of the High Energy Accelerator Research (KEK) in Tukuba, Japan. The methodology in synchrotron scattering experiments has been described elsewhere (Takeno 2016). Scattered intensity from X-ray with a wavelength of 1.5 Å was detected with PILATUS 1 M and 100 K for SAXS and WAXS measurements, respectively. The scattered images were circularly averaged to obtain the scattering curves as a function of the magnitude of the wavevector q.(Ilavsky 2012; Shimizu et al. 2016) The

SAXS intensity was corrected for the incident beam, background scattering and transmission, and reduced to absolute units.(Zhang et al. 2010).

Self-healing

We checked the ability of the self-healing for the gel sheet prepared in the above manner. The gel was cut in the middle of the sheet, and then the self-healing of the cut gel was examined by keeping the cut surface in contact at 25 °C for 24 h in an incubator. To prevent the vaporization of water during the self-healing process, the gel sheet was sandwiched between two pieces of Kapton film, and was placed in a plastic container with a cover, in which high humidity was kept by putting a petri dish full of water. Tensile measurements were conducted for the self-healed gel.

Results and discussion

Characterization of CNF

The XRD profiles for CNF-L, M and S powders are shown in Fig. S1, where crystalline peaks characteristic of cellulose crystals (Park et al. 2010) were observed for all the profiles. We estimated crystallinity of CNF-L, M and S from their XRD curves, so that their crystallinities were 0.65 (for CNF-L), 0.49 (CNF-M) and 0.55 (CNF-S). Furthermore, SEM was used to observe the morphology of CNF (Fig. S2). We show the SEM images of CNF samples dried on a copper grid in Fig. S2 in the Supplementary Material. Although their fibers are somewhat aggregated, the fiber length of CNF-L, CNF-M and CNF-S appear to be approximately > 20 μm, 5–10 μm and $\sim$ 1 μm, respectively.

Mechanical properties of hydrogels

Firstly, let us show the mechanical properties of CNF-M/PVA and CNF-M/PVA/borax hydrogels in order to clarify the effect of borax on the mechanical properties of CNF/PVA hydrogels. Since the CNF-M/PVA hydrogels have comparatively good properties in both tensile strength and stretchability as shown later, they are appropriate to investigate the effect of borax. Figure 1 presents tensile stress–strain curves of CNF-M/PVA hydrogels prepared in the FT method without borax (a) and with it (b) at various CNF-M concentrations. The tensile stress for the CNF-M/PVA gels without and with borax increased with the increase of the CNF-M concentrations, indicating that CNF-M plays a significant role in enhancement of the mechanical strength. As a matter of fact, the CNF-M/PVA/borax gel is robust, e.g., 2 wt% CNF-M/PVA/borax gel with a thickness of 1 mm is able to lift a weight of $\sim$ 1 kg (Fig. 2). The Young's modulus E, the fracture stress σ_f and the fracture strain ε_f are shown in Fig. 3a–c. For CNF-M/PVA gels without borax, both E and σ_f became larger with the increase of the CNF-M concentrations, whereas ε_f monotonously decreased. On the whole, extensibility for CNF-M/PVA hydrogels was low ($< 350\%$), though the Young's modulus reached $\sim$ 1 MPa at 4 wt% CNF-M. In the case of CNF-M/PVA hydrogels containing borax, addition of borax significantly improved extensibility, e.g., the extensibility of the PVA/borax gel without CNF-M attained the value larger than 1000%, whereas that of the gel containing CNF-M was $\sim$ 600%. Addition of CNF-M improved the tensile strength, which reached the maximum value of $\sim$ 0.94 MPa at 2 wt% CNF-M, indicating that CNF-M made a great contribution to reinforcement of the PVA/borax hydrogel. The reinforcement effect of CNF on the elongation of the hydrogel is caused by the interaction between CNF and PVA, or the complexation between borax and CNF as shown later. On the other hand, the lowering of the elongation accompanied by addition of CNF may result from the increase in the structural inhomogeneity in the gel.

Next, we investigated the effect of the fiber length of CNF on the tensile properties of PVA/borax hydrogels prepared in the FT method. Figure 4 depicts the tensile stress–strain curves (a), the Young's modulus E (b), the fracture stress σ_f (c) and the fracture strain ε_f (d) for CNF/PVA/borax gel at different CNF fiber lengths. The gels using CNF with shorter fiber length (CNF-S) were highly stretchable, and the extensibility attained the values higher than 1000% at all CNF-S concentrations covered in this study. Contrary to this, the Young's modulus for CNF/PVA gels with longer fiber length was higher, whereas the extension was not high much in comparison with that of CNF-S/PVA/borax gels. These results may arise from difference in dispersion of CNF, i.e., the dispersion of CNF in CNF-S/PVA/borax gels may be comparatively homogeneous, whereas that of CNF-L/

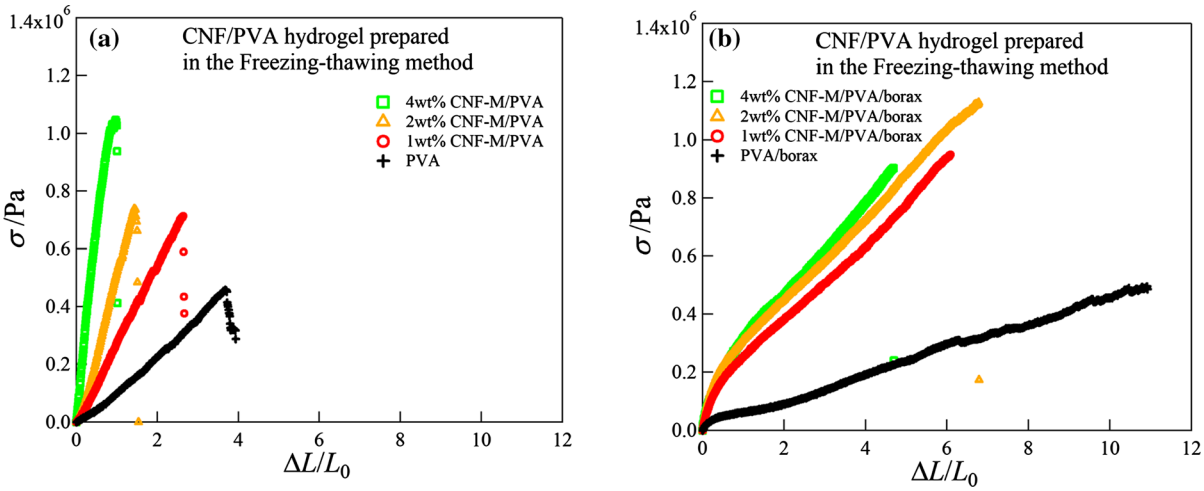

Fig. 1 Representative stress–strain curves for CNF/PVA hydrogels (**a**) and for CNF/PVA/borax hydrogels (**b**) at different CNF-M concentrations

Fig. 2 Pictures of a weight of ∼ 1 kg (left) and 2 wt% CNF-M/PVA/borax gel that lifts the weight (right)

PVA/borax gels may be inhomogeneous, because they are difficult to disperse CNF.

Wide angle X-ray scattering and Fourier transform infrared spectroscopy

Figure 5 presents WAXS profiles for PVA hydrogels with and without borax, and for 2 wt% CNF-M/PVA/borax hydrogels. All the WAXS curves had a peak at q = 1.38 Å^{-1}, which corresponds to overlapping of (101) and (10$\bar{1}$) Bragg peaks from crystallites of PVA (Huan et al. 2016; Kanaya et al. 1994). The peak areas for PVA/borax, and CNF-M/PVA/borax hydrogels were smaller than that of the PVA hydrogel without borax (see magnification around the (101) and (10$\bar{1}$) Bragg peaks in Fig. 5b). The WAXS curves for the freeze-dried samples also show the similar behavior, i.e., the peak for the hydrogel containing borax is broader than that of the hydrogel without borax (see Fig. S3 in the supporting information). These results suggest that cross-linking between PVA and borax tends to suppress crystallization of PVA. A small peak at $q \approx 1.59$ Å^{-1} in Fig. 5a was observed only for PVA hydrogel containing CNF-M, which corresponds to reflection from (200) plane of cellulose I_β crystals (Huan et al. 2016; Zhang et al. 2014). Thus, the WAXS measurements have shown that CNF/PVA hydrogels are reinforced by the PVA crystallites and the rigid cellulose crystalline fibers.

FT-IR measurements were performed to elucidate the interactions between constituent molecules. Figure 6a presents FT-IR spectra of CNF-M, PVA, and CNF-M/PVA, which do not contain borax. Large and broad peaks were observed at 3362 cm^{-1}, which was assigned to O–H stretching vibration of hydroxy groups that forms intermolecular hydrogen bonds (Han et al. 2017). We confirmed intermolecular hydrogen bonds in the CNF-M/PVA composite hydrogel according to the method by Peresin et al. (2010), i.e., the spectrum obtained by subtracting the spectrum of PVA from that of CNF-M/PVA was compared with the spectrum of CNF-M, where a scale factor was used on the basis of the adsorption of PVA at 850 cm^{-1} (see the arrows in Fig. 6a). On the whole, the subtracted spectrum is similar to that of CNF-M, e.g., absorption peaks for both systems were observed at 3335 and 3287 cm^{-1} as shown in Fig. 6b, which is similar to the result by Gentile et al. (2018).

When we take a close look at the spectra, the subtracted spectrum was somewhat broader than that

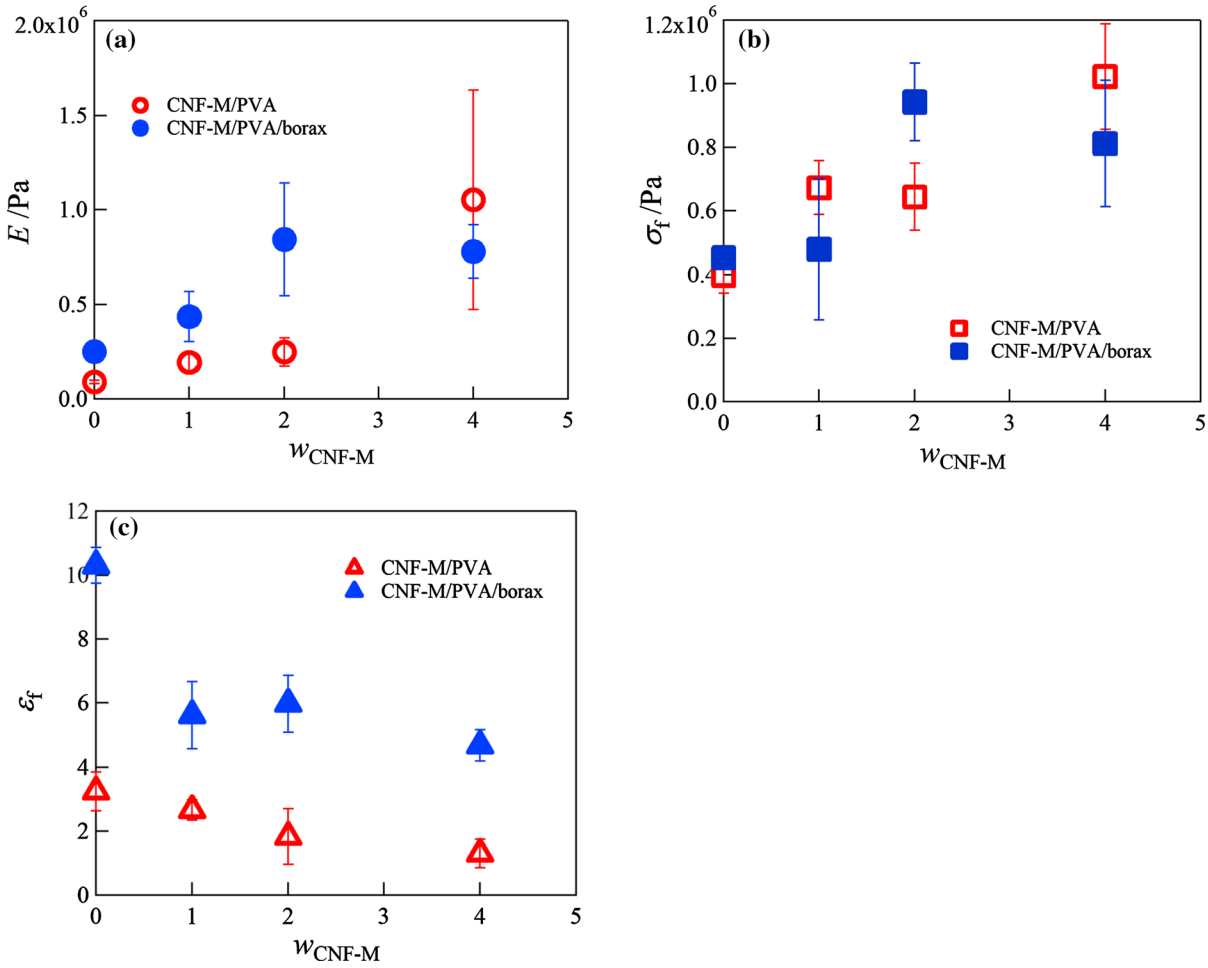

Fig. 3 The Young's modulus (**a**), the fracture stress (**b**) and the fracture strain (**c**) for CNF/PVA hydrogels without and with borax at different CNF-M concentrations

of CNF-M, which may suggest the existence of hydrogen bonds between hydroxyl groups of CNF-M and PVA. Figure 7a depicts FT-IR spectra of CNF-M/borax, PVA/borax, and CNF-M/PVA/borax. Several peaks characteristic of the presence of borate were observed at 660 (bending of B–O–B linkages within borate networks), 830 (B–O stretching from residual $B(OH)_4^-$), 1333 and 1416 cm^{-1} (asymmetric stretching relaxation of B–O–C) (Spoljaric et al. 2014). The peaks at 1333 and 1416 cm^{-1} suggest that two types of complexation between hydroxy groups and borate is formed for both systems of PVA/borax and CNF-M/borax, i.e., the former peak corresponds to tetrahedral complexation, whereas the latter peak indicates formation of trigonal complexation (Fig. 7b) (Kobayashi and Kitaoka 1997; Spoljaric et al. 2014). Thus, WAXS and IR results have clarified that a dual cross-linking by micro crystallites of PVA arising from the FT process and by complexation between PVA (or CNF) and borate form the network of the composite gel.

Structure of CNF/PVA hydrogels cross-linked by freezing/thawing method and borax

First we present SEM images for CNF-M/PVA and CNF-M/PVA/borax hydrogels in Fig. 8. The hydrogel containing borax shows a three-dimensional network morphology with small voids, which are formed by removal of water arising from freeze-drying. Also the images suggest that CNF somewhat aggregates in the composite gel.

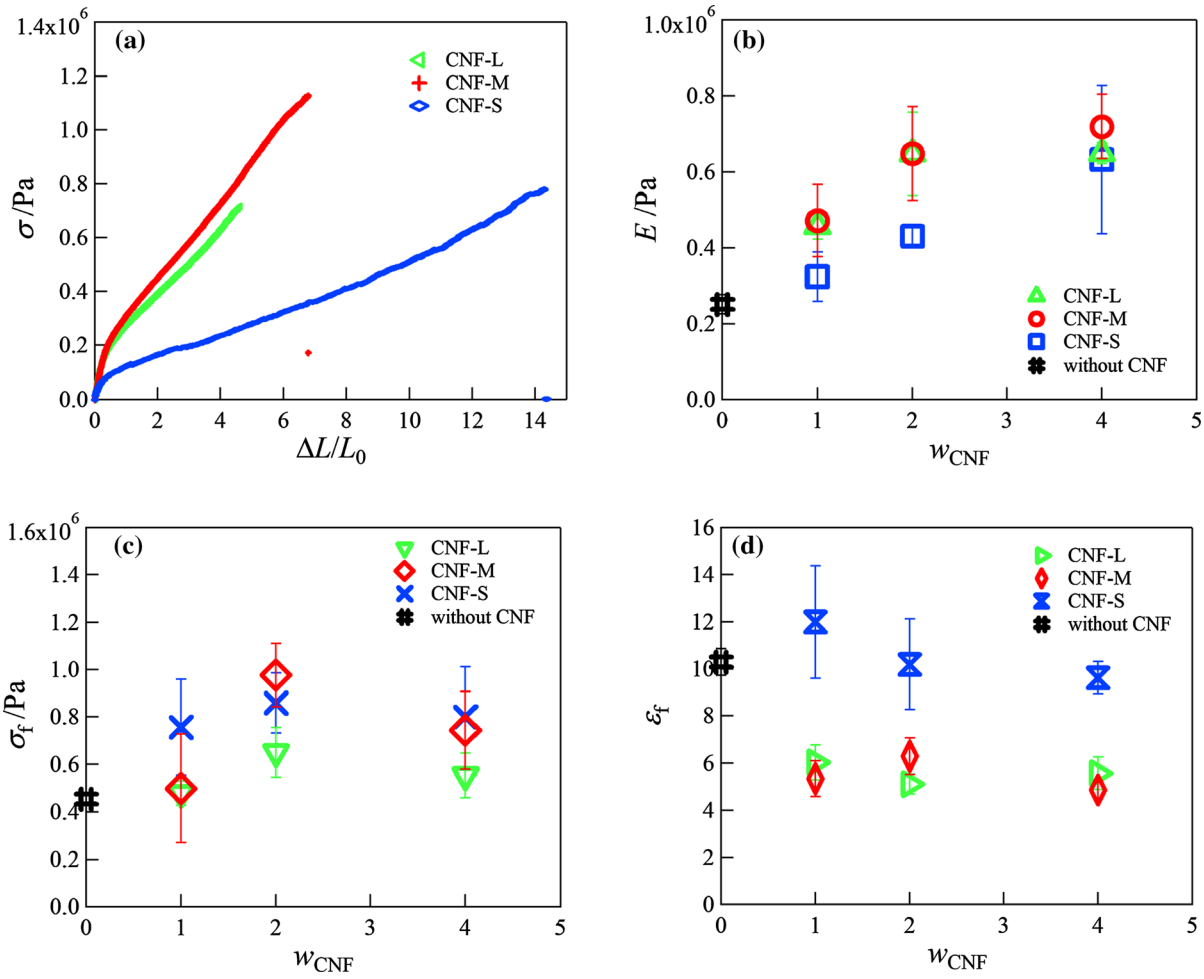

Fig. 4 Representative stress–strain curves for 2 wt% CNF/PVA/borax hydrogels with different fiber length (**a**), the Young's modulus (**b**), the fracture stress (**c**) and the fracture strain (**d**) at different CNF concentrations

We investigated structures of CNF/PVA hydrogels cross-linked by microcrystals of PVA and complexation between borate and hydroxy groups using synchrotron SAXS. The scattering intensity $I(q)$ from monodisperse particles can be expressed as a function of the magnitude of the wave vector q as follows (Takeno 2016; Wang 2004),

$$I(q) = KP(q)S(q), \tag{1}$$

where q is defined by

$$q = \frac{4\pi \sin\frac{\theta}{2}}{\lambda}. \tag{2}$$

Here, λ and θ are the wavelength of X-ray and the scattering angle, respectively. $P(q)$ and $S(q)$ are the form factor of the particles and the structure factor, respectively. K is a prefactor of the scattering intensity.

Figure 9 shows SAXS profiles for PVA and PVA/borax hydrogels prepared in the FT method. The scattering intensity for the gel containing borax was much lower at small q in comparison with the gel without borax. This result suggests that the inhomogeneity in the gel is greatly suppressed by complexation between the hydroxy groups and borate. The structure of PVA hydrogel has been investigated by many researchers, and the crystallites has a layered structure.(Hassan and Peppas 2000a) As the PVA hydrogels are composed of crystalline and amorphous regions, we shall consider the structural model composed of polymer crystals forming lamellar stacks and amorphous polymers in this analysis. In the case of

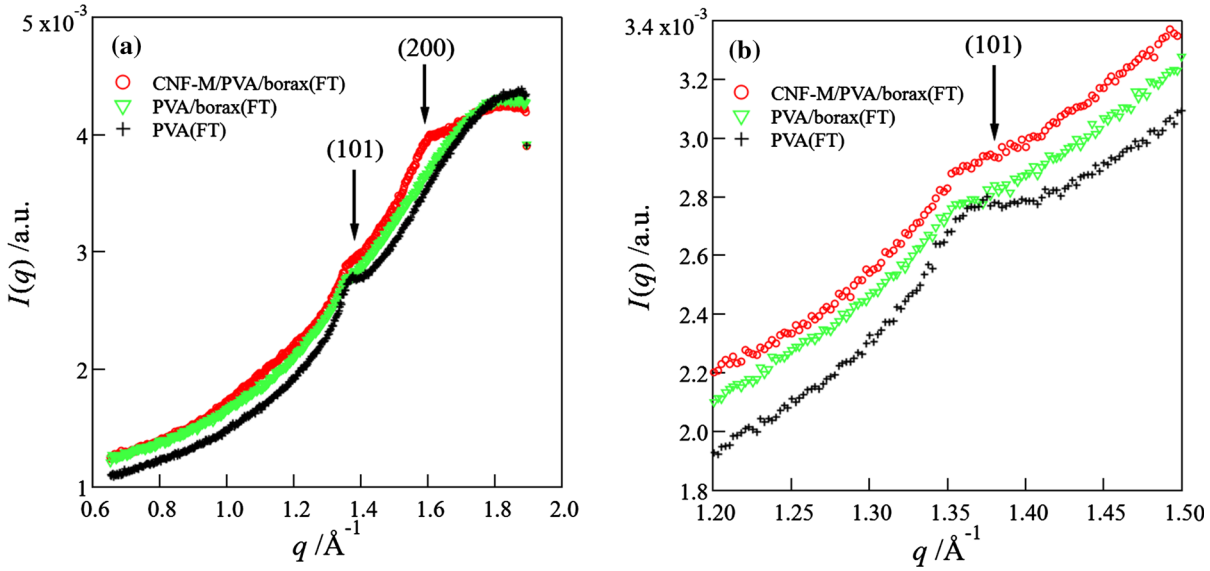

Fig. 5 WAXS curves (**a**) and the magnification (**b**) for PVA, PVA/borax and 2 wt% CNF-M/PVA/borax hydrogels

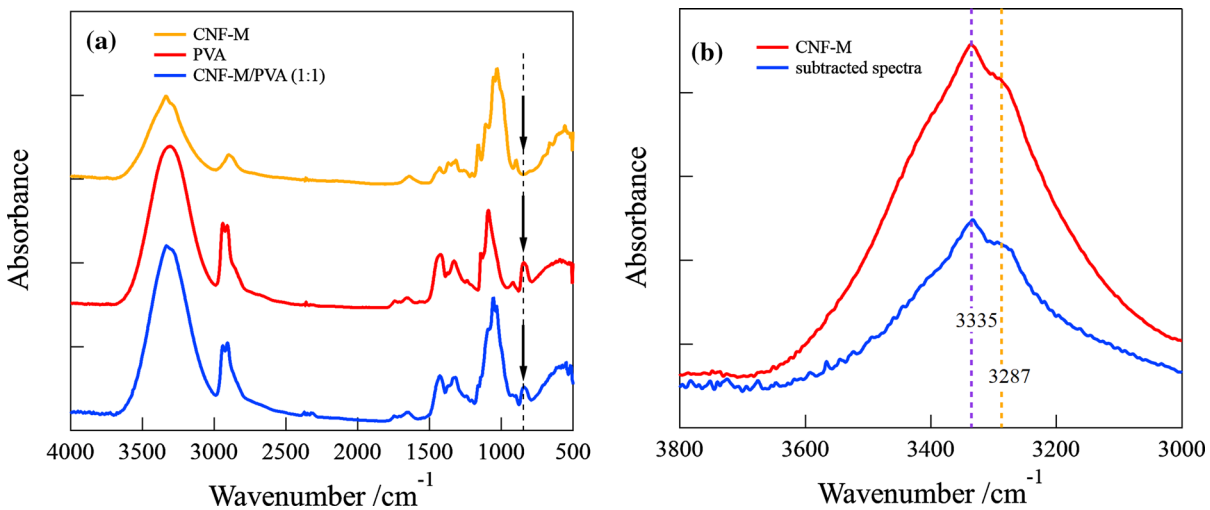

Fig. 6 FT-IR spectra for CNF-M, PVA, CNF-M/PVA(1:1) (**a**), and FT-IR spectra subtracted the PVA spectrum from that of the CNF/PVA and for CNF-M (**b**)

lamellar crystals having the lamella thickness L_c, $P(q)$ is described by (Glatter and Kratky 1982)

$$P(q) \sim \frac{1}{q^2}\left[\frac{L_c sin(qL_c/2)}{qL_c/2}\right]^2. \quad (3)$$

On the other hand, the structure factor for an infinite number of lamellae is expressed by (Richter et al. 1997; Wang 2004)

$$S(q) = \frac{\sinh\left(q^2\sigma_{L_l}^2/4\right)}{\cosh\left(q^2\sigma_{L_l}^2/4\right) - cos(qL_l)}, \quad (4)$$

where L_l is the periodicity of a one-dimensional paracrystalline lattice, and σ_{L_l} is the standard deviation of the L_l. The scattering intensity from the amorphous region may be described by the Ornstein–Zernike form.

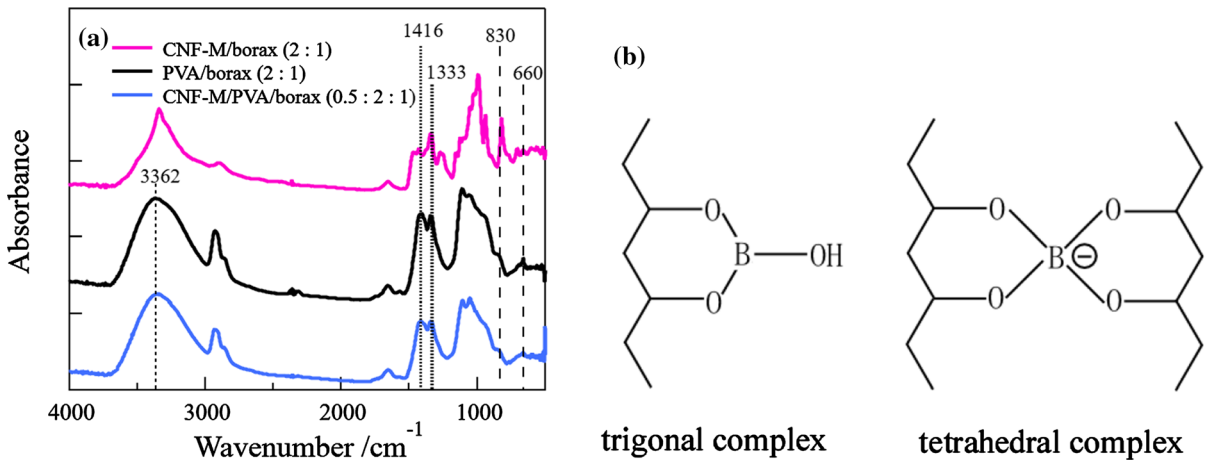

Fig. 7 FT-IR spectra for CNF-M/borax, PVA/borax and CNF-M/PVA/borax (**a**) and structure of complexation between hydroxy groups of PVA and borate (**b**)

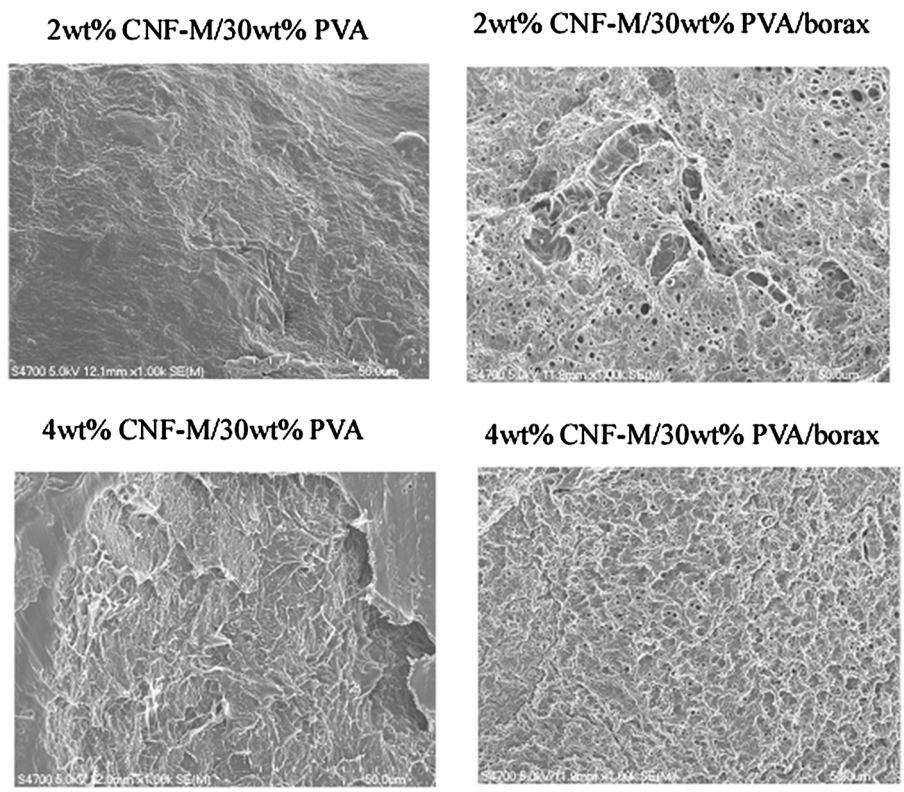

Fig. 8 SEM images for CNF-M/PVA/borax, and CNF-M/PVA hydrogels

$$I(q) = \frac{I(0)}{1 + \xi^2 q^2} \tag{5}$$

Here ξ and $I(0)$ represent the correlation length and the scattering intensity at $q = 0$, respectively.

We analyzed the scattering intensity curves for PVA and PVA/borax hydrogels using Eqs. (1)–(5). The fitted curves are presented in Fig. 9, and the obtained parameters are summarized in Table 1. The values of the parameters for both gels are close except

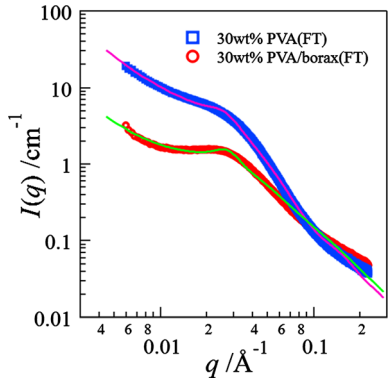

Fig. 9 Small-angle X-ray scattering intensity curves for PVA hydrogels with and without borax

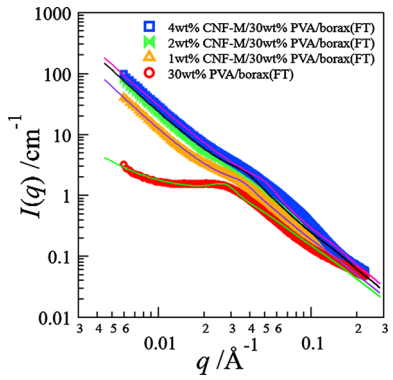

Fig. 10 Small-angle X-ray scattering intensity curves for CNF-M/PVA/borax hydrogels at various CNF-M concentrations

for the correlation length. The correlation length for the PVA/borax gel was much smaller than that of the PVA gel, which suggests that the inhomogeneity in the gel is suppressed due to the cross-linking between borax and PVA.

Figure 10 depicts SAXS profiles for CNF-M/PVA/borax gels at various CNF-M concentrations. These SAXS curves also have a small and broad peak or a shoulder around $q = 0.035 \sim 0.05$ Å^{-1}, implying that PVA forms lamella crystal in the CNF-M/PVA/borax hydrogels as well as PVA/borax hydrogels. The scattering curves for CNF-M/PVA/borax gels exhibit a power-law behavior with an exponent at low q. The power-law behavior comes from the scattering of cellulose nanofibers. The Beaucage unified model has been used to analyze the scattering curves from the multilevel structures with the power-law behavior (Beaucage 1995, 1996, 2004; Beaucage et al. 2004; Beaucage and Schaefer 1994). The model smoothly describes the transition between the power-law behavior at high q and the Guinier behavior at low q as follows,

$$I(q) = G\exp\left(-\frac{q^2R_g^2}{3}\right) + B\left[erf\left(\frac{qR_g}{\sqrt{6}}\right)\right]^{3p} q^{-p}, \quad (6)$$

where the prefactors G and B have the following relation,

$$B = \frac{Gp}{R_g^p \Gamma\left(\frac{p}{2}\right)} \quad (7)$$

R_g is the radius of gyration of a structure at a given level, and p is the exponent of the power-law scattering. $\Gamma(p/2)$ is the gamma function. We analyzed the scattering data for CNF-M/PVA/borax gels with the combination of Eqs. (1)–(7). As there are too many parameters in Eqs. (1)–(7), we fixed the parameters of the O–Z equation and the lamella thickness in this analysis, where we used the parameters obtained in the fitting analysis of PVA/borax gels. The solid curves in Fig. 10 are the best fits according to Eqs. (1)–(7). The scattering curves do not level off at low q and therefore it is difficult to estimate R_g from these curves (Takeno et al. 2012). Thus, we estimated L_l,σ_{L_l} and p from the fitting analysis. The results are presented in Table 2. The values of the exponents ($p = 2.26 \sim 2.42$) much larger than the exponent of 1, which represents the scattering behavior from rod particles ($I(q) \sim q^{-1}$), were obtained for all CNF-M/PVA/borax gels. This

Table 1 The result of the parameters obtained in the fitting analysis for PVA and PVA/borax gels

Sample	L_c/Å	L_l/Å	σLl/Å	ξ/Å
PVA gel (FT)	58 ± 11	190 ± 16	113 ± 17	64 ± 36
PVA/borax gel (FT)	61 ± 43	203 ± 23	91 ± 24	25 ± 10

Table 2 The result of the parameters obtained in the fitting analysis for CNF-M/PVA/borax gels at various CNF-M concentrations

Sample	L_l/Å	σLl/Å	p
4 wt% CNF-M/PVA/borax gel (FT)	109 ± 27	53 ± 12	2.26 ± 0.06
2 wt% CNF-M/PVA/borax gel (FT)	143 ± 36	72 ± 17	2.33 ± 0.09
1 wt% CNF-M/PVA/borax gel (FT)	151 ± 49	76 ± 25	2.42 ± 0.18

result suggests that the cellulose nanofibers somewhat aggregate in the gel.

Self-healing behavior of CNF/PVA hydrogels cross-linked by freezing/thawing method and borax

Self-heling behavior was examined for the 2 wt% CNF-M/PVA/borax hydrogel. The hydrogel with a dumbbell shape was cut into two pieces, and immediately the cut surface was brought into contact (Fig. 11a). After the hydrogel was placed for 24 h at 25 °C in an incubator, the tensile test was carried out. Figure 11b depicts typical stress–strain curves for the self-healed 2 wt% CNF-M/PVA/borax and PVA/borax gels. For comparison, the tensile curves for the uncut gels are also shown in the graph. The figures show that both CNF-M/PVA/borax and PVA/borax hydrogels possess self-healing behavior. The self-healing behavior of 35% PVA hydrogel prepared in a FT method has been reported by Zhang et al. (2012) Their result showed that the fracture stress of the hydrogel after 48 h healing attained ∼ 200 kPa which corresponds to ∼ 72% of the stress of the original uncut hydrogel, whereas the fracture strain achieved ∼ 2.8 (280% elongation). Our study has

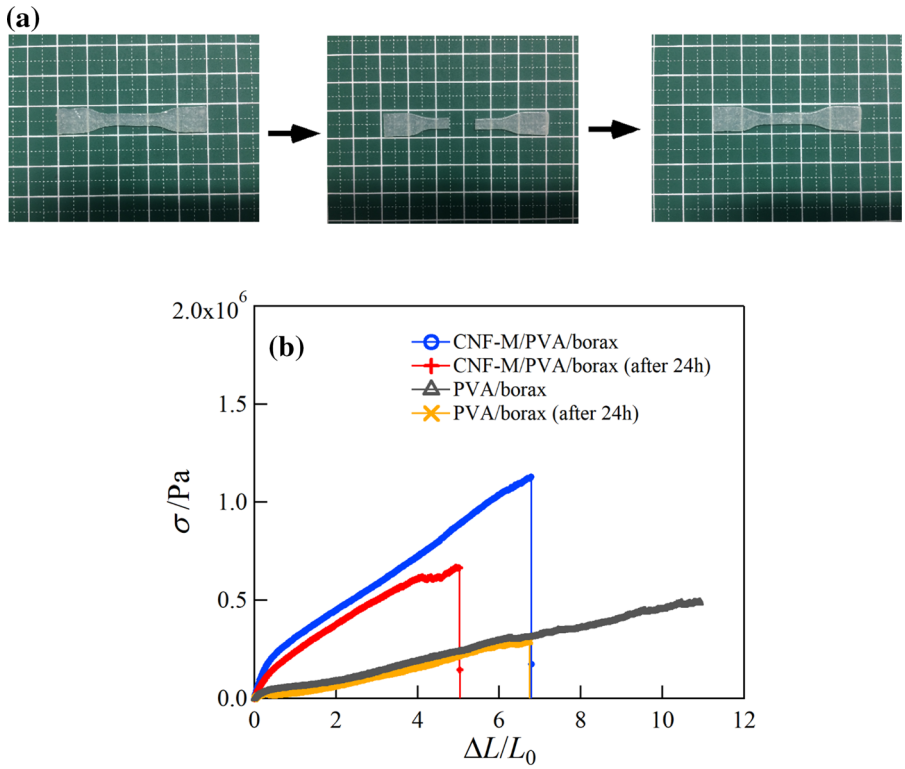

Fig. 11 Pictures of an original CNF-M/PVA/borax hydrogel (left), the hydrogel cut into two pieces (middle) and the hydrogel brought into contact after being cut (right) (**a**). Representative stress–strain curves for the self-healed gels and the uncut gels (**b**)

shown that the CNF/PVA hydrogels cross-linked by both the FT method and borax also possess a self-heling ability. The fracture stress and strain of PVA/borax gel after 24 h healing attained 350 kPa and 6.6 (660% elongation), respectively, whereas those of the CNF-M/PVA/borax gel after 24 h healing were 590 kPa and 4.4 (440% elongation) (see Table 3). Thus, the self-healed gels were quite stretchable and robust, although their elongations and tensile strength became somewhat lower than those of the uncut gels. Thus it has been confirmed that the self-healing ability is maintained, even if borax and CNF is added to the PVA gel prepared in the FT method.

Structural model for CNF/PVA hydrogels cross-linked by freezing/thawing method and borax

As mentioned above, structures of CNF/PVA/borax hydrogels were examined by FT-IR and simultaneous SAXS/WAXS techniques. Schematic illustration of the structures of CNF/PVA/borax hydrogels based upon these results is presented in Fig. 12. These results have clarified that the PVA/borax hydrogels are multiply cross-linked by the trigonal and tetrahedral complexations between the hydroxy groups and borate, hydrogen bonds between hydroxy groups, and the lamella crystals of PVA. Although the complexation has a tendency to decrease degree of crystallinity of PVA, the tensile strength of the PVA/borax hydrogel is higher than that of the PVA hydrogels due to the multiple cross-linking. In addition, the SAXS results have shown that the PVA-borate complexation suppresses the structural inhomogeneity of the hydrogel, so that the degree of extensibility for the hydrogel has been greatly improved. Thus, it is important to disperse the cross-linking points for improvement of the mechanical performance of the hydrogels, as has been confirmed by other systems (Takeno and Sato 2016). Addition of CNF to the PVA/borax hydrogel does not affect the degree of crystallinity of PVA (see Fig. S4 in the supporting information). On the other hand, FT-IR measurements have confirmed that complexation between CNF and borate is formed. As a matter of fact, addition of borax to the CNF-M dispersions highly enhances the viscoelasticity, e.g., the CNF-M/borax does not flow by inversion of the vial for a short time (10 min), although the CNF-M dispersion without borax flows (see Fig. S5 in the supporting information). Accordingly, the mechanical strength has been considerably enhanced by addition of CNF to PVA/borax gels. Thus, it can be concluded that CNF successfully works as a filler of PVA/borax hydrogels.

Conclusion

We investigated mechanical properties and structures of CNF/PVA hydrogels cross-linked by borax and micro crystals of PVA that were formed in the FT process. FT-IR experiments have confirmed two-types of complexation between hydroxy groups of PVA (or CNF) and borate, i.e., trigonal and tetrahedral complexations. The complexations lessened the degree of the crystallinity of PVA, and suppressed the structural inhomogeneity in the gel. As a result, not only the mechanical strength but also the extensibility of the gels was considerably improved in comparison with the gel without borax. Addition of CNF to the PVA/borax hydrogel caused new crosslinks (or interactions) such as complexations between hydroxy groups of CNF and borate, and hydrogen bonds between PVA and CNF, so that the tensile stress has been greatly enhanced. In addition, it was found that the mechanical performance significantly depends upon the size of CNF. CNF/PVA/borax gels with shorter fiber length are highly stretchable, e.g., they show extensibility higher than 1000%, whereas the reinforcement effect is more effective for the CNF/PVA/borax gels with longer fiber length.

Table 3 Tensile properties of the self-healed gel

Sample	E/kPa	σ_f/kPa	ε_f
CNF-M/PVA/borax (uncut gel)	$(8.4 \pm 3.0) \times 10^2$	$(9.4 \pm 1.2) \times 10^2$	6.0 ± 0.9
CNF-M/PVA/borax (self-healed gel)	$(6.0 \pm 0.3) \times 10^2$	$(5.9 \pm 0.8) \times 10^2$	4.4 ± 0.4
PVA/borax (uncut gel)	$(2.5 \pm 0.2) \times 10^2$	$(4.5 \pm 0.2) \times 10^2$	10.3 ± 0.6
PVA/borax (self-healed gel)	$(2.3 \pm 0.1) \times 10^2$	$(3.5 \pm 1.3) \times 10^2$	6.6 ± 0.7

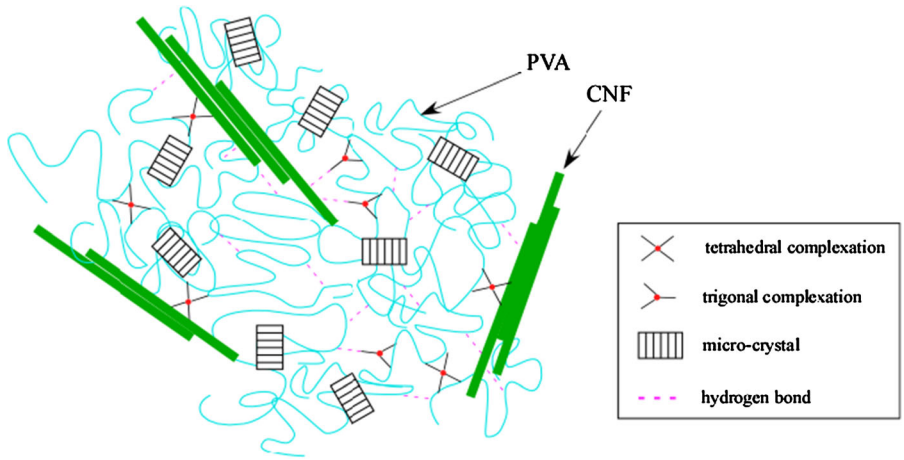

Fig. 12 Schematic representation of a structural model for CNF/PVA/borax hydrogels

Acknowledgments This work was supported by JSPS KAKENHI Grant No. 19K05594. The synchrotron SAXS/WAXS measurements were conducted under the approval of Photon Factory Program Advisory Committee. The XRD measurements were performed at the Center for Instrumental Analysis of Gunma University, and we thank Mr. Sakamoto of the Center for his technical assistance of the measurements.

References

Avolio R, Bonadies I, Capitani D, Errico ME, Gentile G, Avella M (2012) A multitechnique approach to assess the effect of ball milling on cellulose. Carbohydr Polym 87:265–273. https://doi.org/10.1016/j.carbpol.2011.07.047

Avolio R et al (2015) Effect of cellulose structure and morphology on the properties of poly(butylene succinate-*co*-butylene adipate) biocomposites. Carbohydr Polym 133:408–420. https://doi.org/10.1016/j.carbpol.2015.06.101

Bauer S, Bauer-Gogonea S, Graz I, Kaltenbrunner M, Keplinger C, Schwodiauer R (2014) 25th anniversary article: a soft future: from robots and sensor skin to energy harvesters. Adv Mater 26:149–162. https://doi.org/10.1002/adma.201303349

Beaucage G (1995) Approximations leading to a unified exponential power-law approach to small-angle scattering. J Appl Crystallogr 28:717–728. https://doi.org/10.1107/S0021889895005292

Beaucage G (1996) Small-angle scattering from polymeric mass fractals of arbitrary mass-fractal dimension. J Appl Crystallogr 29:134–146. https://doi.org/10.1107/S0021889895011605

Beaucage G (2004) Determination of branch fraction and minimum dimension of mass-fractal aggregates. Phys Rev E. https://doi.org/10.1103/Physreve.70.031401

Beaucage G, Schaefer DW (1994) Structural studies of complex-systems using small-angle scattering—a unified Guinier power-law approach. J Non-Cryst Solids 172:797–805. https://doi.org/10.1016/0022-3093(94)90581-9

Beaucage G, Kammler HK, Pratsinis SE (2004) Particle size distributions from small-angle scattering using global scattering functions. J Appl Crystallogr 37:523–535. https://doi.org/10.1107/S0021889804008969

Boyaci T, Orakdogen N (2016) Poly(*N*, *N*-dimethylaminoethyl methacrylate-*co*-2-acrylamido-2-methyl-propanosulfonic acid)/Laponite nanocomposite hydrogels and cryogels with improved mechanical strength and rapid dynamic properties. Appl Clay Sci 121–122:162–173. https://doi.org/10.1016/j.clay.2015.12.018

Chen D, Pei QB (2017) Electronic muscles and skins: a review of soft sensors and actuators. Chem Rev 117:11239–11268. https://doi.org/10.1021/acs.chemrev.7b00019

Cong HL, Radosz M, Towler BF, Shen YQ (2007) Polymer-inorganic nanocomposite membranes for gas separation. Sep Purif Technol 55:281–291. https://doi.org/10.1016/j.seppur.2006.12.017

De France KJ, Hoare T, Cranston ED (2017) Review of hydrogels and aerogels containing nanocellulose. Chem Mater 29:4609–4631. https://doi.org/10.1021/acs.chemmater.7b00531

Gentile G, Cocca M, Avolio R, Errico M, Avella M (2018) Effect of microfibrillated cellulose on microstructure and properties of poly(vinyl alcohol) foams. Polymers 10:813. https://doi.org/10.3390/polym10080813

Glatter O, Kratky O (1982) Small angle X-ray scattering. Academic Press, London

Golmohammadi H, Morales-Narvaez E, Naghdi T, Merkoci A (2017) Nanocellulose in sensing and biosensing. Chem Mater 29:5426–5446. https://doi.org/10.1021/acs.chemmater.7b01170

Han J et al (2017) Effects of nanocellulose on the structure and properties of poly(vinyl alcohol)-borax hybrid foams. Cellulose 24:4433–4448. https://doi.org/10.1007/s10570-017-1409-4

Hassan CM, Peppas NA (2000a) Structure and applications of poly(vinyl alcohol) hydrogels produced by conventional crosslinking or by freezing/thawing methods. Adv Polym Sci 153:37–65

Hassan CM, Peppas NA (2000b) Structure and morphology of freeze/thawed PVA hydrogels. Macromolecules 33:2472–2479. https://doi.org/10.1021/Ma9907587

Hoffman AS (2012) Hydrogels for biomedical applications. Adv Drug Deliv Rev 64:18–23. https://doi.org/10.1016/j.addr.2012.09.010

Holloway JL, Lowman AM, Palmese GR (2013) The role of crystallization and phase separation in the formation of physically cross-linked PVA hydrogels. Soft Matter 9:826–833. https://doi.org/10.1039/c2sm26763b

Huan SQ, Bai L, Cheng WL, Han GP (2016) Manufacture of electrospun all-aqueous poly(vinyl alcohol)/cellulose nanocrystal composite nanofibrous mats with enhanced properties through controlling fibers arrangement and microstructure. Polymer 92:25–35. https://doi.org/10.1016/j.polymer.2016.03.082

Huang M, Hou Y, Li Y, Wang D, Zhang L (2017) High performances of dual network PVA hydrogel modified by PVP using borax as the structure-forming accelerator. Des Monomers Polym 20:505–513. https://doi.org/10.1080/15685551.2017.1382433

Ilavsky J (2012) Nika: software for two-dimensional data reduction. J Appl Crystallogr 45:324–328. https://doi.org/10.1107/S0021889812004037

Kanaya T, Ohkura M, Kaji K, Furusaka M, Misawa M (1994) Structure of poly(vinyl alcohol) gels studied by wide-angle and small-angle neutron-scattering. Macromolecules 27:5609–5615. https://doi.org/10.1021/Ma00098a014

Kaneko F, Seto N, Sasaki K, Sakurai S, Kimura T (2013) Simultaneous SAXS and WAXS study on the guest exchange process of syndiotactic polystyrene: crystalline complex formation with triethylene glycol dimethyl ether. Macromol Chem Phys 214:1893–1900. https://doi.org/10.1002/macp.201300001

Kobayashi M, Kitaoka Y (1997) Complex formation of boric acids with di- and tricarboxylic acids and poly(vinyl alcohol) in aqueous solutions. Macromol Symp 114:303–308. https://doi.org/10.1002/masy.19971140141

Lee H et al (2017) Enhancement of mechanical properties of polymeric nanofibers by controlling crystallization behavior using a simple freezing/thawing process. RSC Adv 7:43994–44000. https://doi.org/10.1039/c7ra06545k

Narita T, Mayumi K, Ducouret G, Hébraud P (2013) Viscoelastic properties of poly(vinyl alcohol) hydrogels having permanent and transient cross-links studied by microrheology, classical rheometry, and dynamic light scattering. Macromolecules 46:4174–4183. https://doi.org/10.1021/ma400600f

Park S, Baker JO, Himmel ME, Parilla PA, Johnson DK (2010) Cellulose crystallinity index: measurement techniques and their impact on interpreting cellulase performance. Biotechnol Biofuels 2:3. https://doi.org/10.1186/1754-6834-3-10

Peppas NA (1975) Turbidimetric studies of aqueous poly(vinyl-alcohol) solutions. Makromol Chem 176:3433–3440

Peresin MS, Habibi Y, Zoppe JO, Pawlak JJ, Rojas OJ (2010) Nanofiber composites of polyvinyl alcohol and cellulose nanocrystals: manufacture and characterization. Biomacromolecules 11:674–681. https://doi.org/10.1021/bm901254n

Rath T et al (2014) Real time X-ray scattering study of the formation of ZnS nanoparticles using synchrotron radiation. Mater Chem Phys 144:310–317. https://doi.org/10.1016/j.matchemphys.2013.12.045

Richter D et al (1997) Polymer aggregates with crystalline cores: The system polyethylene-poly(ethylenepropylene). Macromolecules 30:1053–1068. https://doi.org/10.1021/Ma961039k

Shimizu N, Yatabe K, Nagatani Y, Saijyo S, Kosuge T, Igarashi N (2016) Software development for analysis of small-angle X-ray scattering data. AIP Conf Proc 1741:050017

Spoljaric S, Salminen A, Luong ND, Seppälä J (2014) Stable, self-healing hydrogels from nanofibrillated cellulose, poly(vinyl alcohol) and borax via reversible crosslinking. Eur Polym J 56:105–117. https://doi.org/10.1016/j.eurpolymj.2014.03.009

Stauffer SR, Peppas NA (1992) Poly(vinyl alcohol) hydrogels prepared by freezing-thawing cyclic processing. Polymer 33:3932–3936. https://doi.org/10.1016/0032-3861(92)90385-A

Takeno H (2016) Synchrotron small-angle X-Ray scattering and small-angle neutron scattering studies of nanomaterials. In: Kumar CSSR (ed) X-ray and neutron techniques for nanomaterials characterization. Springer, Berlin, pp 717–760

Takeno H, Nakamura W (2013) Structural and mechanical properties of composite hydrogels composed of clay and a polyelectrolyte prepared by mixing. Colloid Polym Sci 291:1393–1399. https://doi.org/10.1007/s00396-012-2871-z

Takeno H, Kimura Y (2016) Molecularweight effects on tensile properties of blend hydrogels composed of clay and polymers. Polymer 85:47–54. https://doi.org/10.1016/j.polymer.2016.01.008

Takeno H, Sato C (2016) Effects of molecular mass of polymer and composition on the compressive properties of hydrogels composed of Laponite and sodium polyacrylate. Appl Clay Sci 123:141–147. https://doi.org/10.1016/j.clay.2016.01.030

Takeno H, Maehara A, Yamaguchi D, Koizumi S (2012) A Structural study of an organogel investigated by small-angle neutron scattering and synchrotron small-angle X-ray scattering. J Phys Chem B 116:7739–7745. https://doi.org/10.1021/jp3008514

Takeno H, Yanagita M, Motegi Y, Kondo S (2015) Relationship between helical aggregates and polymorphs in a 12-hydroxystearic acid gel: their thermal stability and formation kinetics. Colloid Polym Sci 293:199–207

Vashist A et al (2018) Nanocomposite hydrogels: advances in nanofillers used for nanomedicine. Gels 4:75. https://doi.org/10.3390/gels4030075

Wang H (2004) Time-resolved small-angle neutron scattering study of polyethylene crystallization from solution. J Polym Sci Pol Phys 42:3133–3147. https://doi.org/10.1002/polb.20181

Wang L, Ishihara S, Hikima Y, Ohshima M, Sekiguchi T, Sato A, Yano H (2017) Unprecedented development of ultra-high expansion injection-molded polypropylene foams by introducing hydrophobic-modified cellulose nanofibers. ACS Appl Mater Inter 9:9250–9254. https://doi.org/10.1021/acsami.7b01329

Xu XZ, Liu F, Jiang L, Zhu JY, Haagenson D, Wiesenborn DP (2013) Cellulose nanocrystals vs. cellulose nanofibrils: a comparative study on their microstructures and effects as

polymer reinforcing agents. Acs Appl Mater Inter 5:2999–3009. https://doi.org/10.1021/am302624t

Zhang F, Ilavsky J, Long GG, Quintana JPG, Allen AJ, Jemian PR (2010) Glassy carbon as an absolute intensity calibration standard for small-angle scattering. Metall Mater Trans A 41A:1151–1158. https://doi.org/10.1007/s11661-009-9950-x

Zhang H, Xia H, Zhao Y (2012) Poly(vinyl alcohol) hydrogel can autonomously self-heal. ACS Macro Letters 1:1233–1236. https://doi.org/10.1021/mz300451r

Zhang W, He X, Li C, Zhang X, Lu C, Zhang X, Deng Y (2014) High performance poly (vinyl alcohol)/cellulose nanocrystals nanocomposites manufactured by injection molding. Cellulose 21:485–494. https://doi.org/10.1007/s10570-013-0141-y